Investigation of the Radiation Mechanism of Heatsinks Based on Characteristic Mode Theory

Xu Wang, *Student Member, IEEE*, Matthew Wu, Jagan Rajagopalan, Akshay Mohan, Donghyun Kim, *Member, IEEE*, and Chulsoon Hwang, *Senior Member, IEEE*

***Abstract*—Heatsinks may cause radiated emission and radio frequency interference problems when they are mounted on printed circuit boards. In this article, the radiation mechanism of heatsinks is systematically investigated using characteristic mode theory. The dipole moment is a commonly used equivalent source model for integrated circuits that drive radiated emission from heatsinks. On the basis of a simplified modal weighting coefficient formulation, the interactions between the dipole moment and the significant modes of the heatsink are efficiently evaluated, thus providing a clear physical insight into noise source placement. Finally, the grounding post design, a commonly used EMI mitigation method, is also discussed. The relative error of the mode-based field prediction is less than 3 dB compared with the full-wave simulation.**

***Index Terms*—Characteristic mode, dipole moment, electromagnetic interference (EMI) mitigation, grounding design, heatsink, radiation mechanism.**

I. Introduction

AS THE integration density of integrated circuits (ICs) and electronic systems continues to increase, system power consumption is also dramatically increasing, thus making heatsinks a critical component for heat dissipation [1]. However, heatsinks also cause substantial electromagnetic interference (EMI) problems because of their relatively large electric sizes [2], [3].

The radiation mechanism of heatsinks has long been studied. In [4], analytical formulas have been proposed to relate the maximum radiated emission (RE) to the voltage between the heatsink and ground plane. The far-field RE is then predicted on the basis of the equivalent magnetic current in the cavity region and the monopole-antenna current approximation on the tall heatsink body. This approximation is valid only for heatsinks with a relatively simple shape. Recently, several studies have been conducted to investigate the effects of heatsink geometry [5], [6], [7]. A more accurate model than monopole antennas is needed to reflect geometric variations in an EMI risk assessment.

TABLE I
Literature Review of CMA Application in EMC Community

Topic	Literature
Mitigation of EMI using absorbing material	[8]
Radiation from cubic heatsink	[9]
Radiation hotspot Analysis based on eigencurrent distribution	[10]
Experimental verification of CMA using reverberation chamber	[11]
Out-of-band coupling between antennas	[12]

As summarized in Table I, the characteristic mode theory has been used to study the coupling and radiation mechanisms. Heatsinks have also been studied with characteristic mode analysis (CMA) in previous works [8], [9]. The results in [8] have shown that heatsink resonance can be accurately predicted with the CMA approach, on the basis of comparison with measurements of the total radiated power (TRP). In [9], CMA has been used to simulate a cubic heatsink and to investigate multiple grounding designs based on the modal current distribution. The effectiveness of CMA has also been validated by TRP simulation. Because the TRP of each mode depends on the power intensity integrated over the entire sphere (far-field region) [10], whether CMA can be used to accurately predict the near-field and far-field emissions generated in a specific region/direction remains an open question.

Generally, heatsinks absorb energy from noisy digital ICs [3], [13]. However, the detailed IC information is generally not available to electromagnetic compatibility (EMC) engineers; therefore, the equivalent source reconstruction method is commonly used to model the radiation of digital circuits [14], [15], [16]. The dipole moment model is the most commonly used equivalent radiation source for the IC structure because it represents the current paths that cause emission problems [17]. For example, a magnetic dipole has been extracted in [16] to represent the RE from the bonding wires of a digital IC. However, to the best of authors' knowledge, no comprehensive analysis of the interaction between the dipole moment source and the heatsink has been reported in the literature.

The purpose of this article is threefold.

1) Verify the validity of using the CMA approach to predict the near-field and far-field emissions from the heatsink,

Manuscript received 8 February 2023; revised 2 June 2023; accepted 29 June 2023. This work was supported by the National Science Foundation under Grant IIP-1916535. *(Corresponding author: Chulsoon Hwang.)*

Xu Wang, Donghyun Kim, and Chulsoon Hwang are with EMC Laboratory, Missouri University of Science and Technology, Rolla, MO 65409 USA (e-mail: xw7dh@mst.edu; dkim@mst.edu; hwangc@mst.edu).

Matthew Wu, Jagan Rajagopalan, and Akshay Mohan are with the Wireless Technology Group of Amazon Lab126, Sunnyvale, CA 94089 USA (e-mail: menghsi@amazon.com; rrajagop@lab126.com; aksmohan@lab126.com).

Color versions of one or more figures in this article are available at https://doi.org/10.1109/TEMC.2023.3297553.

Digital Object Identifier 10.1109/TEMC.2023.3297553

which are essential for radio frequency interference (RFI) estimation and RE prediction. (The criterion for selecting significant modes for interference prediction is also discussed. More stringent criterion than that used by the antenna research community is needed.)
2) Model the interaction between the dipole moment model and the characteristic modes of the heatsink.
3) Discuss several mitigation methods based on modal analysis, including noise source placement and grounding design.

The rest of this article is organized as follows. In Section II, characteristic mode theory is briefly revisited. A partition-based emission prediction strategy is subsequently introduced and used to relate the resultant field to a specific geometry (current path). In addition, formulas for calculating the interaction between the general reconstructed noise source and the characteristic modes are presented. In Section III, validation of emission risk prediction by using the modal fields is conducted. In Section IV, the selection of critical modes and the mitigation methods based on modal analysis are further discussed, and a plate heatsink is used as an example. Finally, Section V concludes this article.

II. Theory Background

A. Theory of Characteristic Mode

The characteristic mode currents [18] are derived from a generalized eigenvalue equation

$$\mathbf{X}\mathbf{J}_n = \lambda_n \mathbf{R}\mathbf{J}_n \tag{1}$$

where $\mathbf{J}_n$ is the nth modal current, and $\mathbf{R}$ and $\mathbf{X}$ are the real and imaginary parts of the impedance matrix $\mathbf{Z}$, respectively

$$\mathbf{Z} = \mathbf{R} + j\mathbf{X}. \tag{2}$$

Because the modal currents form a weighted orthogonal set over the surface of the conductor body, the induced current on the object, $\mathbf{J}$, can be expressed as a linear superposition of the modal currents when the heatsink is subjected to external excitation

$$\mathbf{J} = \sum_{n=1}^{N} \alpha_n \mathbf{J}_n \tag{3}$$

where $\mathbf{J}_n$ is the nth modal current, and N is the mode number used to expand the currents. N could be a small number for an object of electrically intermediate size [18]. The modal weighting coefficient (MWC), α_n, can be calculated as

$$\alpha_n = \frac{< \mathbf{E}_{\text{inc}}, \mathbf{J}_n >}{1 + j\lambda_n} \tag{4}$$

where $\mathbf{E}_{\text{inc}}$ denotes the incident field from the external source, and the inner product $<>$ is taken over the entire object.

Owing to the linear nature of Maxwell's equations, the scattered field can be represented by a linear combination of the modal patterns

$$\mathbf{E} = \sum_{n=1}^{N} \alpha_n \mathbf{E}_n \tag{5}$$

where $\mathbf{E}_n$ is the modal near field or far field produced by the modal current $\mathbf{J}_n$.

Of note, the half-space green's function, rather than the free-space green's function, must be used here to calculate the impedance matrix to account for the infinite large plane approximation for the large printed circuit board plane [4].

B. Dipole Moment as Excitation

In the original article on characteristic mode theory, Harrington discussed and presented MWC formulations with infinitesimal dipole sources as excitations [18, (34) and (35)]. However, this case has received less attention than the delta gap voltage source and the plane wave source cases, which are widely used for antenna performance and scattering analysis [12], [19]. In the EMC research community, dipole moments are widely used as equivalent noise sources for the IC and other components in RFI and RE prediction [13], [14], [20]. For instance, the dipole moment model has been used to develop an effective RFI mitigation strategy by rotating the noise source [21]. This section revisits the MWC formulation for the dipole moment excitation case, which can serve as a practical noise source for a heatsink [3], [21].

Here, we study the interaction between the magnetic dipole and the modal currents of the heatsink. The case of an electric dipole can be handled similarly. On the basis of the reaction concept, the Rayleigh–Carson reciprocity theorem indicates the sensibility of the heatsink modal currents by the dipole source [22]

$$\int_V -(\mathbf{H}_n \cdot \mathbf{M})dV = \int_V (\mathbf{E} \cdot \mathbf{J}_n)dV \tag{6}$$

where $\mathbf{J}_n$ and $\mathbf{H}_n$ denote the nth modal current and its radiated H field, respectively, $\mathbf{M}$ and $\mathbf{E}$ represent the magnetic dipole source (noise source) and its E field, respectively, and V is the entire space. Of note, the dipole moment is defined only at a discrete point in the space; thus

$$-\mathbf{H}_n(r_0) \cdot \mathbf{M} = \int_V (\mathbf{E} \cdot \mathbf{J}_n)dV \tag{7}$$

where r_0 is the location of the dipole source.

After substitution of the inner product in (4) with $-\mathbf{H}_n(r_0) \cdot \mathbf{M}$, the MWC for a single magnetic dipole excitation becomes

$$\alpha_n = -\frac{\mathbf{M} \cdot \mathbf{H}_n(r_0)}{1 + j\lambda_n}. \tag{8}$$

Now the MWC depends only on the eigenvalue, the magnitude of the dipole moment, and the modal H field at a particular location, but not on the integral over the surface of the heatsink. This simplified formulation is not only a valid alternative to the MWC calculation, but also provides an intuitive explanation of the interaction between the noise source and the modal currents.

C. Partition-Based Emission Prediction Method

Geometric differences in heatsinks may result in different EMI risks [6]. To demonstrate whether CMA can be used to accurately predict the emission from a specific geometry, such

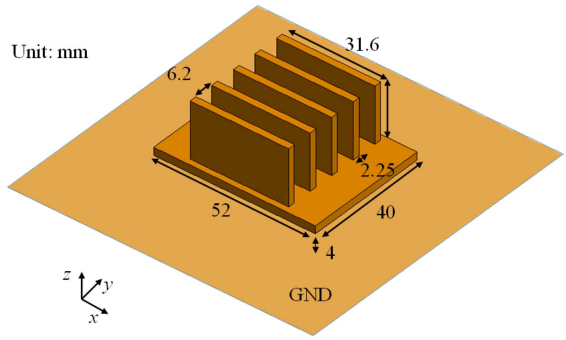

(a)

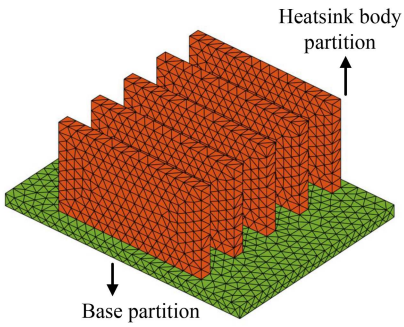

(b)

Fig. 1. Plate heatsink and the partitioning procedure. (a) Geometry of the heatsink. (b) Base partition and heatsink body partition.

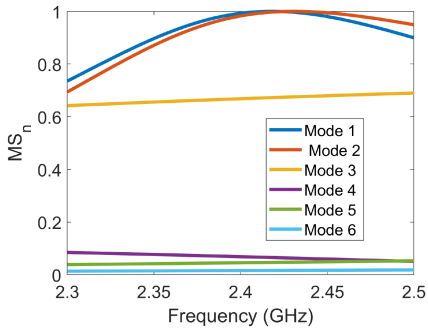

Fig. 2. Modal significance spectrum between 2.3 and 2.5 GHz.

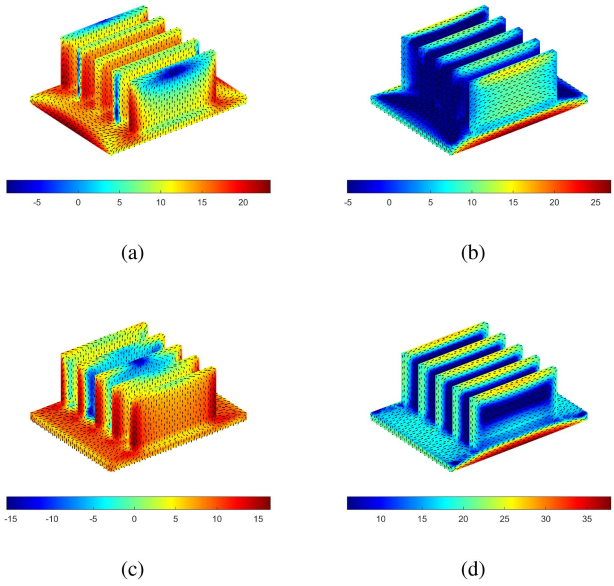

(a) (b) (c) (d)

Fig. 3. Modal current distribution at 2.4 GHz. Units: dBA/m. (a) Mode 1. (b) Mode 2. (c) Mode 3. (d) Mode 4.

as the plates on a heatsink body, a partition-based approach is used.

Because the operator connecting the current and its resultant field is linear [23, (3.25)], the radiated fields from the entire structure can be decomposed into the contributions from different geometry partitions

$$\mathbf{E}(\mathbf{r}) = \mathbf{E}_{S_1}(\mathbf{r}) + \mathbf{E}_{S_2}(\mathbf{r}) \tag{9}$$

where S_1 denotes the base partition surface, and S_2 denotes the heatsink body partition surface, as shown in Fig. 1(b). $\mathbf{E}(\mathbf{r})$, $\mathbf{E}_{S_1}(\mathbf{r})$, and $\mathbf{E}_{S_2}(\mathbf{r})$ denote the radiated fields due to the currents on the entire structure, the currents on the base partition, and the currents on the body partition, respectively. The formulas used to calculate the near field and far field for arbitrary current distribution can be found in [23] and are not repeated herein.

The partitioning procedure is a simple yet efficient and effective postprocessing procedure to understand the contributions from different current paths. If necessary, it can also be used to study the emission of an individual pin of a pin-type heatsink or an individual plate of a plate heatsink.

III. Validation

A. CMA for a Plate Heatsink

In this section, the plate heatsink structure in Fig. 1(a) is analyzed by using CMA from 2.3 to 2.5 GHz, wherein its emission can be picked up by a Wi-Fi antenna. The heatsink sits above a large printed circuit board ground plane, and the gap between the base and the ground plane is 4 mm. The largest length of the triangular cell is set as 3 mm ($\lambda/40$), which is sufficient to capture the behavior of the high-order modes.

The modal significance ($\mathrm{MS}_n = |1/(1+j\lambda_n)|$) spectrum for the first six modes is shown in Fig. 2. The modal currents are shown in Fig. 3. Two resonant modes are observed, and the results for 2.4 GHz are analyzed in the rest of this article. The modal currents on the base partition of the first and second modes correlate with the typical TM_{10} and TM_{01} modes of a rectangular cavity. For the heatsink body partition, the currents also differ for the two modes: a vertical monopole-like current is observed for mode 1, and a horizontal monopole-like current is observed for mode 2 on the plates. In particular, for mode 4, both vertical and horizontal current components are presented along the edges of the plates.

Fig. 4 shows the modal far field for modes 1, 2, and 4. The differences in the radiation lobes can be attributed to the difference in the modal currents (base and body partition). To

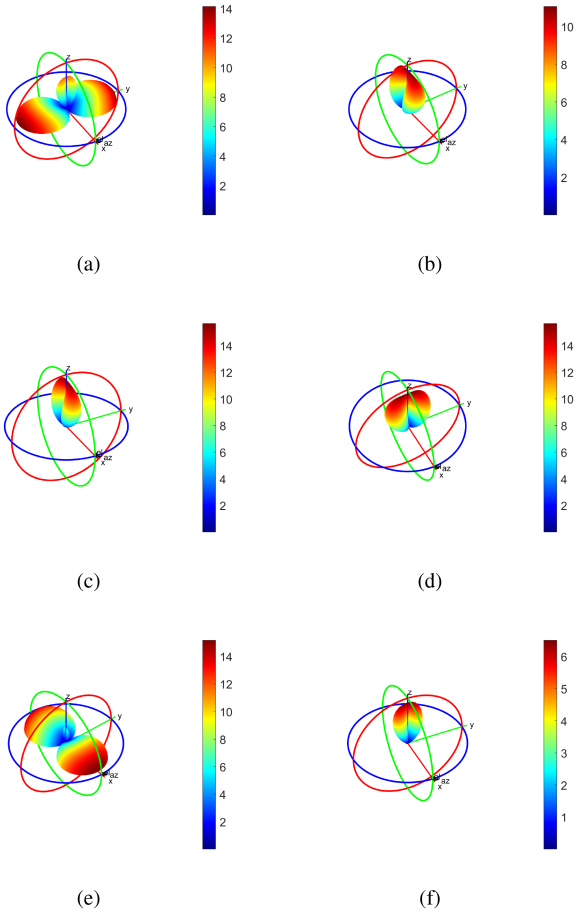

Fig. 4. Modal far-field pattern. Units: V/m. (a) E_θ, mode 1. (b) E_ϕ, mode 1. (c) E_θ, mode 2. (d) E_ϕ, mode 2. (e) E_θ, mode 4. (f) E_ϕ, mode 4.

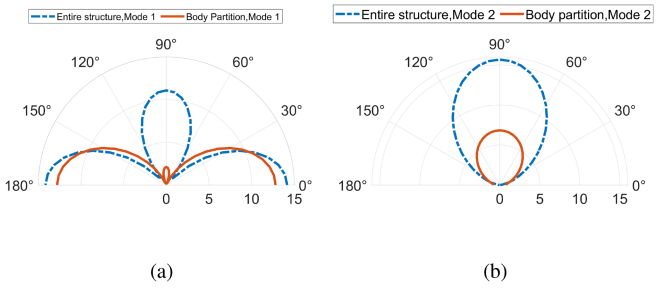

Fig. 5. Comparison of 2-D cut of modal far field. Units: V/m. (a) E_θ component of mode 1 ($\phi = 90$ and $\phi = 270$ planes). (b) E_θ component of mode 2 ($\phi = 0$ and $\phi = 180$ planes).

support our hypothesis, the partitioning procedure is applied for modes 1 and 2. The RE from the entire structure and the heatsink body is compared in Fig. 5. The vertical current component on the heatsink body in mode 1 can be concluded to introduce a main lobe in the horizontal directions, while both horizontal current components on the base and heatsink body in mode 2 produce lobes toward the $\theta = 90^\circ$ direction (XY plane). In addition, the contribution of the heatsink body partition can be quantified; for instance, the horizontal lobe in mode 1 is 13 V/m

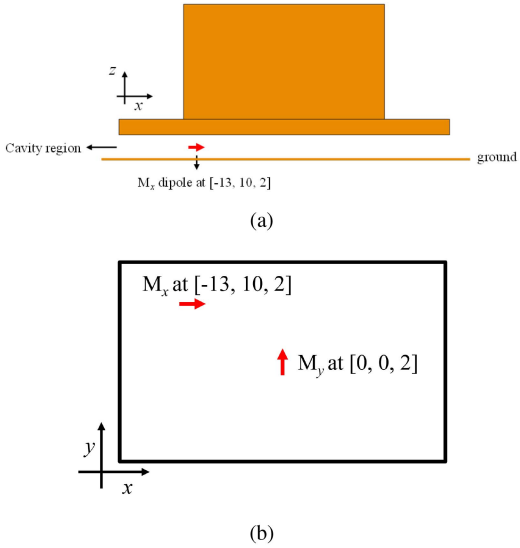

Fig. 6. Full-wave simulation configuration. Excitation I: Mx dipole at [−13 mm, 10 mm, 2 mm]. Excitation II: My dipole at [0 mm, 0 mm, 2 mm]. (a) Side view. (b) Bottom view.

TABLE II
MWC COMPARISON FOR MX DIPOLE EXCITATION

Mode Index	λ_n	$\lvert Hx \rvert$	$\lvert \alpha_n \rvert$ (using 8)	$\lvert \alpha_n \rvert$ (FEKO)
1	-0.122	3.853	3.825	3.825
1	-0.189	0.032	0.032	0.032
2	-1.11	0.435	0.291	0.291
3	14.59	0.195	0.013	0.013
4	22.1	3.07	0.139	0.139

and is the main contributor to the radiation along the horizontal direction.

B. Interaction Between the Noise Source and Characteristic Modes

To verify whether CMA can be used for EMI risk prediction (i.e., prediction of the field levels at the near-field region of interest and far-field direction of interest) when a noise source is present, an x-direction-oriented magnetic dipole (Mx dipole) is placed at [−13 mm, 10 mm, 2 mm] to mimic the radiation of an IC structure [16]. For simplicity, the magnitude of the magnetic dipole is set to 1 V · m, which is much larger than the realistic case (0.0026 V · m for the bonding wires' RE in [16]).

The simulation configuration is shown in Fig. 6. The MWC can be calculated from (8), on the basis of the eigenvalue and the modal Hx component of each mode (shown in Fig. 7). The MWC comparison with FEKO [using (4)], as given in Table II, indicates a good correlation. Mode 1 is excited because of its larger Hx component.

The current distribution from the full-wave simulation is shown in Fig. 8. Mode 1 is excited. A near-field scanning surface (x from −130 to 130 mm, y from −130 to 130 mm, and $z = 8$ mm) is defined around the heatsink to monitor the near-field emission in the near-field zone. The near-field and far-field emissions based on mode prediction and full-wave simulation are shown in Fig. 9 and Fig. 10, respectively. In this case, the correlation shows

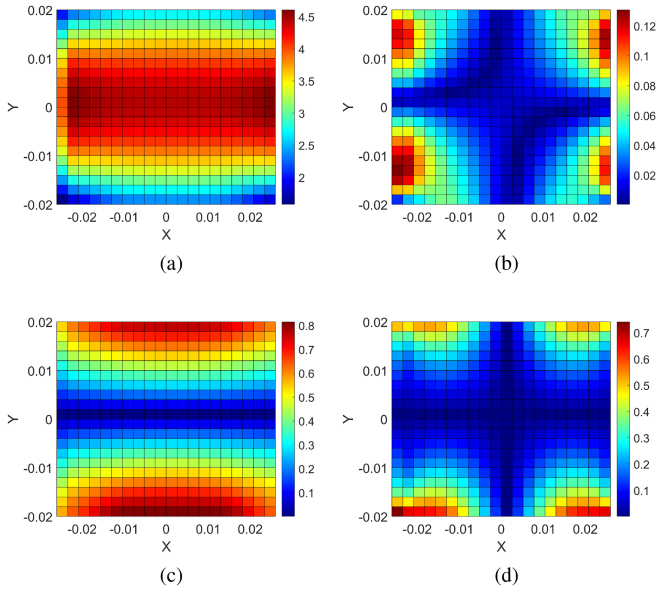

Fig. 7. Modal Hx component in the cavity region at z = 2 mm. Units for field: A/m. Units for coordinates: m. (a) Mode 1. (b) Mode 2. (c) Mode 3. (d) Mode 4.

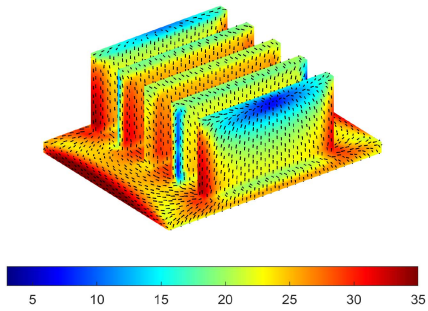

Fig. 8. Current distribution based on full-wave simulation when the heatsink is excited by the Mx dipole. Units: dBA/m.

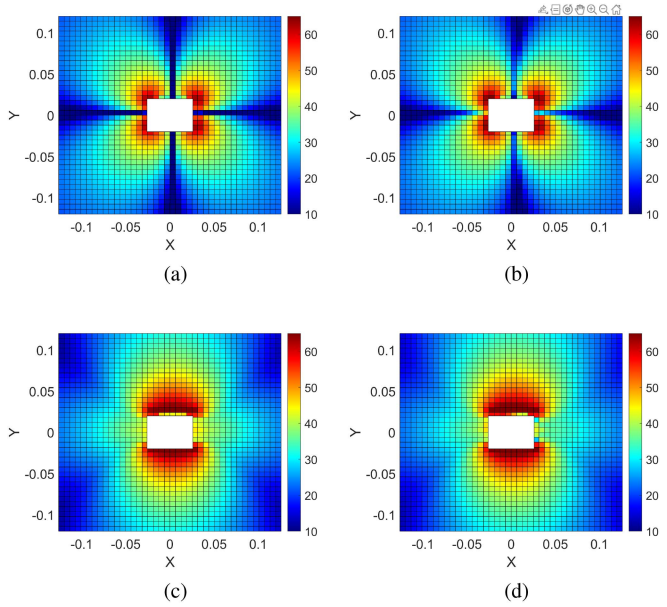

Fig. 9. E-field comparison at the near-field scanning surface between the modal-based prediction and the full-wave simulation when the heatsink is excited by the Mx dipole (the white area in the center is occupied by the heatsink). Units: dBV/m. (a) Ex predicted by $\alpha_1 \mathbf{E}_1$. (b) Ex from full-wave simulation. (c) Ey predicted by $\alpha_1 \mathbf{E}_1$. (d) Ey from full-wave simulation.

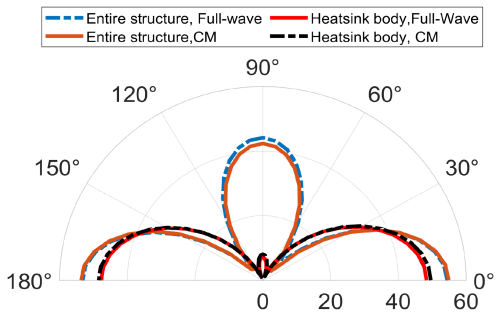

Fig. 10. E_θ component between modal-based prediction ($\alpha_1 \mathbf{E}_1$) and full-wave simulation when the heatsink is subjected to Mx dipole excitation ($\phi = 90$ and $\phi = 270$ planes).

that one significant mode is sufficient to predict the near-field and far-field emission levels with high accuracy.

IV. Discussion

A. Selection of Critical Modes

For conductors of electrically intermediate size, only a few modes are needed to characterize the resultant field of the structure, which are called significant modes. The antenna research community usually defines significant modes by using the modal significance

$$MS_n \begin{cases} \geq 0.707 & \text{significant mode} \\ \leq 0.707 & \text{nonsignificant mode} \end{cases} \tag{10}$$

which is based on the half-power bandwidth of each mode.

For the heatsink case, according to the criteria in (10), mode 4 is nonsignificant and can be ignored. Through the numerical experiment in the following, we show that in some cases ignoring mode 4 can lead to relatively large errors in both the near-field and far-field predictions.

First, the modal Hy pattern in the cavity region is shown in Fig. 11. According to (8), if the modal H field of the nonsignificant mode is sufficiently larger than the significant modes, the nonsignificant modes can also be effectively excited. Therefore, the magnetic dipole is rotated to the y-direction and placed at [0 mm, 0 mm, 2 mm] to excite mode 4. The MWC spectrum is shown in Fig. 12. The magnitude of the MWC of mode 2 is 7.6, and that of mode 4 is 1.47. Both modes 2 and 4 are effectively excited. The vertical component of the induced current of the plates (full-wave simulation result), as shown in Fig. 13, also indicates that mode 4 is excited.

As shown in Fig. 14, the Ez component of mode 4 (on the near-field scanning surface) is larger than that of mode 2, thus indicating that ignoring mode 4 may lead to errors in Ez

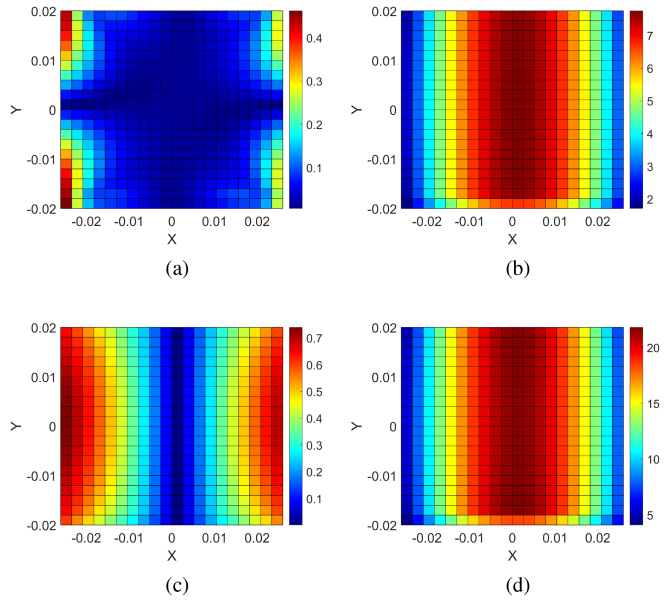

Fig. 11. Modal Hy component in the cavity region. Units: A/m. (a) Mode 1. (b) Mode 2. (c) Mode 3. (d) Mode 4.

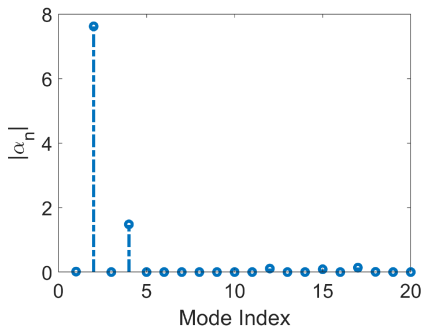

Fig. 12. MWC when the heatsink is excited by the My dipole.

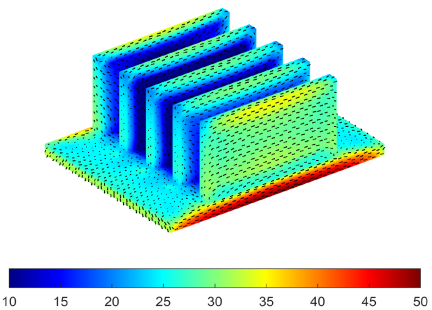

Fig. 13. Current distribution based on full-wave simulation when the heatsink is excited by the My dipole. (Units: dBA/m).

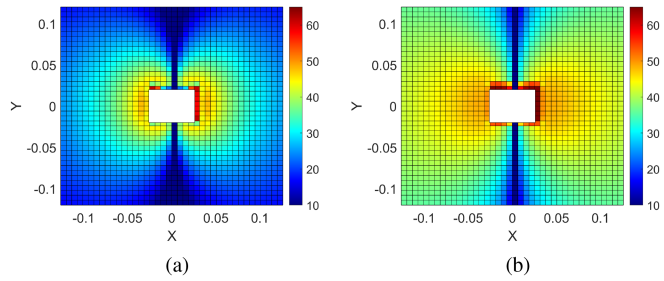

Fig. 14. Modal Ez component on the near-field scanning surface. Units: dBV/m. (a) Mode 2. (b) Mode 4.

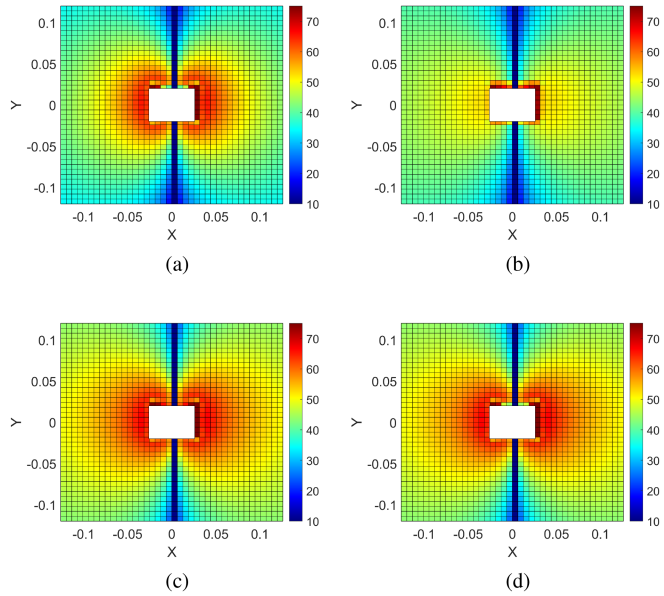

Fig. 15. Ez field prediction at the near-field scanning surface (when the heatsink is excited by the My dipole). Units: dBV/m. (a) $\alpha_2\mathbf{E}_2$. (b) $\alpha_4\mathbf{E}_4$. (c) $\alpha_2\mathbf{E}_2 + \alpha_4\mathbf{E}_4$. (d) Full-wave simulation.

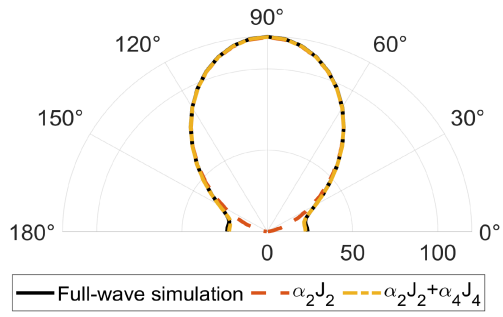

Fig. 16. E_θ comparison when the heatsink is excited by the My dipole ($\phi = 0$ and $\phi = 180$ planes). Units: V/m.

component prediction. The resultant Ez field on the scanned surface, according to different predictions, is shown in Fig. 15. As expected, mode 4 is also a significant contributor to the near-field emission. It is worth mentioning that there is a large discrepancy between the mode-based predictions and the full-wave simulations in the very near region of the heatsink, which is caused by neglecting the higherorder modes. Overall, the relative error is less than 3 dB.

On the other hand, the far-field comparison between the modal-based prediction and the full-wave simulation is shown in Fig. 16. The results show that when only mode 2 is considered, significant errors are observed in the emission risk prediction in the *x*/*y* directions; however, if both modes 2 and 4 are considered, the modal-based approach accurately predicts the far-field

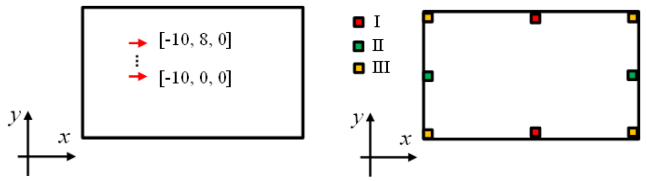

(a) (b)

Fig. 17. Mitigation method experiments. (a) Noise source placement. (b) Grounding designs.

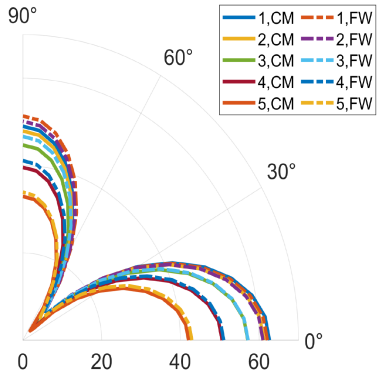

Fig. 18. E_θ at $\phi = 90°$ with different noise source placements. The solid line indicate modal-based predictions, and the dashed lines indicate full-wave simulation results. (Units: V/m).

emission. If the victim is located in the *x*/*y* directions of the heatsink, using only mode 2 for the prediction causes significant errors. In summary, with several critical modes, the modal-based approach can predict the emission risks of a heatsink. However, the criterion used by the antenna research community may not be sufficient for EMI/RFI prediction purposes, especially when interference at a specific direction/region must be considered. Herein, we suggest including more high-order modes for interference prediction, e.g.

$$MS_n \begin{cases} \geq 0.02 & \text{significant mode} \\ \leq 0.02 & \text{nonsignificant mode.} \end{cases} \tag{11}$$

B. Mitigation Method

Noise source placement and grounding posts are two commonly used approaches for RFI/RE mitigation [15], [21], [24]. In this section, these two methods are discussed based on CMA.

1) Noise Source Placement: Because the MWC can be obtained with the modal H field and eigenvalue of each mode, the IC placement method can be studied with the CMA approach. A numerical experiment is used as a proof of concept. As shown in Fig. 17(a), the Mx dipole in the first simulation is swept from (−13 mm, 0 mm, 2 mm) to (−13 mm, 8 mm, 2 mm) with a step size of 2 mm along the *y*-direction. Based on the modal approach, the MWC is first calculated with (8), and then the RE is estimated by multiplication of the MWC with a modal pattern (only mode 1 is used for field prediction). The comparison of the modal-based approach and the full-wave simulation is shown in Fig. 18. A good correlation is achieved for

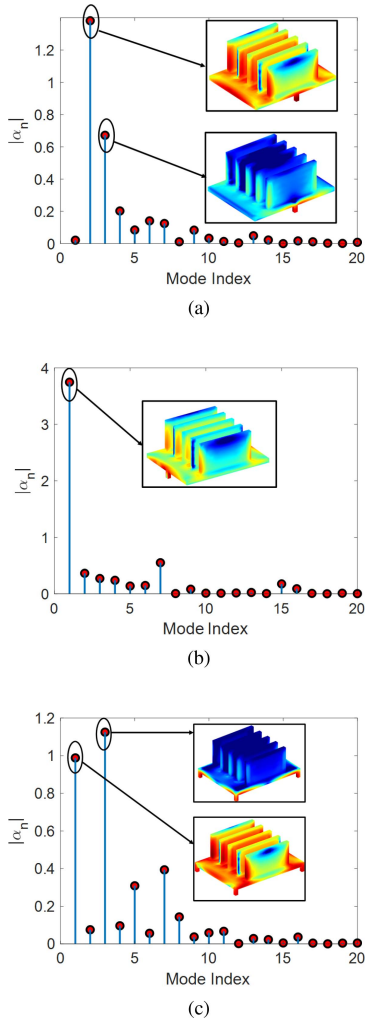

Fig. 19. MWC for different grounding designs when excited by Mx dipole. (a) Design I. (b) Design II. (c) Design III.

the far-field radiation prediction using one significant mode. This numerical experiment demonstrates that the Mx dipole mainly excites the first mode of the heatsink, and the radiation level can be decreased by placing the IC in the weak field region of the first mode. In addition, less than 1 s is required to calculate the final radiation pattern for the modal-based approach, because the MWC calculation is efficient.

2) Grounding Design: Because of the increasing complexity of integration in systems, IC placement is not always feasible for layout engineers to mitigate the EMI/RFI problem. Another popular technique for reducing interference is the use of grounding posts [9], [24]. As shown in Fig. 19, three grounding designs are proposed to study their effectiveness. The CMA is performed, and the MWC excited by the previous Mx dipole at [−13 mm, 10 mm, 2 mm] are shown in Fig. 19. The first mode in the ungrounded heatsink is observed in all the cases: mode 2 in Fig. 19(a), mode 1 in Fig. 19(b), and mode 1 in Fig. 19(c). In addition, new patterns, such as mode 3 in design I [shown in Fig. 19(a)], are presented and excited. In this situation, merely reducing the initial dominant mode (mode 1) does not ensure that interference will be reduced. Algorithms for shape optimization

could be utilized to place grounding posts in the best possible places [25].

V. Conclusion

In this article, characteristic mode theory is utilized to analyze the radiation mechanism of heatsinks. The CMA approach is demonstrated to accurately predict both near-field and far-field interferences. Through use of a partitioning approach, the accuracy of the characteristic modes is verified, and the RE contribution from the heatsink body can be accurately predicted. The simplified MWC formulation for the case of dipole source excitation is revisited and validated, thus not only enabling an intuitive understanding of the interaction between the noise source and heatsink, but also providing a fast and efficient method for IC placement. The method utilized in this work may also be used by the system-level EMC engineers or RF desense engineers and facilitate the analysis of the resonance and interference caused by other metallic housings in the consumer electronic devices. The partition-based RE prediction approach may also be used to study the critical parameter that cause the interference [7]. Further improvements to this study may include a systematic grounding design methodology.

References

[1] C.-T. Chen, C.-K. Wu, and C. Hwang, "Optimal design and control of CPU heat sink processes," *IEEE Trans. Compon. Packag. Technol.*, vol. 31, no. 1, pp. 184–195, Mar. 2008.

[2] H.-W. Shim and T. H. Hubing, "Model for estimating radiated emissions from a printed circuit board with attached cables due to voltage-driven sources," *IEEE Trans. Electromagn. Compat.*, vol. 47, no. 4, pp. 899–907, Nov. 2005.

[3] L. Zhang et al., "Radio-frequency interference estimation for multiple random noise sources," *IEEE Trans. Electromagn. Compat.*, vol. 64, no. 2, pp. 358–366, Apr. 2021.

[4] X. He and T. H. Hubing, "A closed-form expression for estimating the maximum radiated emissions from a heatsink on a printed circuit board," *IEEE Trans. Electromagn. Compat.*, vol. 54, no. 1, pp. 205–211, Feb. 2012.

[5] C. E. Brench, "Heatsink radiation as a function of geometry," in *Proc. IEEE Symp. Electromagn. Compat.*, 1994, pp. 105–109.

[6] H. Dogan, I. B. Basyigit, A. Genc, and S. Helhel, "Parametric study of the radiated emission from the plate-fin CPU heatsink at 2–8 GHz," *IEEE Trans. Electromagn. Compat.*, vol. 62, no. 6, pp. 2401–2410, Dec. 2020.

[7] A. Genc, H. Dogan, I. B. Basyigit, and S. Helhel, "Heatsink preselection chart to minimize radiated emission in broadband on the PCB," *IEEE Trans. Electromagn. Compat.*, vol. 63, no. 2, pp. 419–426, Apr. 2021.

[8] X. Yang et al., "EMI radiation mitigation for heatsinks using characteristic mode analysis," in *Proc. IEEE Symp. Electromagn. Compat., Signal Integrity Power Integrity*, 2018, pp. 374–378.

[9] Q. Wu, H.-D. Bruns, and C. Schuster, "Characteristic mode analysis of radiating structures in digital systems," *IEEE Electromagn. Compat. Mag.*, vol. 5, no. 4, pp. 56–63, Oct.–Dec. 2016.

[10] Y. S. Cao, Y. Wang, L. Jiang, A. E. Ruehli, J. Fan, and J. L. Drewniak, "Quantifying EMI: A methodology for determining and quantifying radiation for practical design guidelines," *IEEE Trans. Electromagn. Compat.*, vol. 59, no. 5, pp. 1424–1432, Oct. 2017.

[11] H. Manoharan, X. Wang, M. Wu, J. Rajagopalan, and C. Hwang, "Experimental verification of characteristic mode analysis (CMA) using reverberation chamber," in *Proc. Asia-Pacific Int. Symp. Electromagn. Compat.*, to be published.

[12] Q. Wu, W. Su, Z. Li, and D. Su, "Reduction in out-of-band antenna coupling using characteristic mode analysis," *IEEE Trans. Antennas Propag.*, vol. 64, no. 7, pp. 2732–2742, Jul. 2016.

[13] Z. Yu, J. A. Mix, S. Sajuyigbe, K. P. Slattery, D. Pommerenke, and J. Fan, "Heat-sink modeling and design with dipole moments representing IC excitation," *IEEE Trans. Electromagn. Compat.*, vol. 55, no. 1, pp. 168–174, Feb. 2013.

[14] Z. Yu, J. A. Mix, S. Sajuyigbe, K. P. Slattery, and J. Fan, "An improved dipole-moment model based on near-field scanning for characterizing near-field coupling and far-field radiation from an IC," *IEEE Trans. Electromagn. Compat.*, vol. 55, no. 1, pp. 97–108, Feb. 2013.

[15] C. Hwang and Q. Huang, "IC placement optimization for RF interference based on dipole moment sources and reciprocity," in *Proc. Asia-Pacific Int. Symp. Electromagn. Compat.*, 2017, pp. 331–333.

[16] M. Ouyang, Y. Sun, J. Lee, J. Kim, and C. Hwang, "Mechanism analysis on radio frequency radiation in IC/package with bonding wires," in *Proc. IEEE Int. Symp. Electromagn. Compat. Signal/Power Integrity*, 2020, pp. 133–138.

[17] Q. Huang, F. Zhang, T. Enomoto, J. Maeshima, K. Araki, and C. Hwang, "Physics-based dipole moment source reconstruction for RFI on a practical cellphone," *IEEE Trans. Electromagn. Compat.*, vol. 59, no. 6, pp. 1693–1700, Dec. 2017.

[18] R. Harrington and J. Mautz, "Theory of characteristic modes for conducting bodies," *IEEE Trans. Antennas Propag.*, vol. 19, no. 5, pp. 622–628, Sep. 1971.

[19] K. Kabalan, R. Harrington, H. Auda, and J. Mautz, "Characteristic modes for slots in a conducting plane, TE case," *IEEE Trans. Antennas Propag.*, vol. 35, no. 2, pp. 162–168, Feb. 1987.

[20] H. Wang, V. Khilkevich, Y.-J. Zhang, and J. Fan, "Estimating radio-frequency interference to an antenna due to near-field coupling using decomposition method based on reciprocity," *IEEE Trans. Electromagn. Compat.*, vol. 55, no. 6, pp. 1125–1131, Dec. 2013.

[21] Q. Huang et al., "A novel RFI mitigation method using source rotation," *IEEE Trans. Electromagn. Compat.*, vol. 63, no. 1, pp. 11–18, Feb. 2021.

[22] J.-M. Jin, *Theory and Computation of Electromagnetic Fields*. Hoboken, NJ, USA: Wiley, 2011.

[23] W. C. Gibson, *The Method of Moments in Electromagnetics*. Boca Raton, FL: Chapman and Hall/CRC, 2021.

[24] X. He and T. H. Hubing, "Mitigation of unintentional radiated emissions from tall VLSI heatsinks using ground posts," *IEEE Trans. Electromagn. Compat.*, vol. 55, no. 6, pp. 1271–1276, Dec. 2013.

[25] B. Yang and J. J. Adams, "Systematic shape optimization of symmetric MIMO antennas using characteristic modes," *IEEE Trans. Antennas Propag.*, vol. 64, no. 7, pp. 2668–2678, Jul. 2016.

Xu Wang (Student Member, IEEE) received the B.S. and M.S. degrees in electrical engineering from the University of Electronic Science and Technology of China, Chengdu, China, in 2015 and 2018, respectively. He is currently working toward the Ph.D. degree in electrical engineering from the Missouri University of Science and Technology, Rolla, MO, USA.

His research interests include partial element equivalent circuit modeling and development of radiation emission models for components and devices.

Matthew Wu received the master's degree in wireless technology from National Chiao Tung University, Hsinchu, Taiwan, in 2011.

He is a Senior RF system/EMC Engineer with Wireless Technology Group, Amazon Lab126, Sunnyvale, CA, USA, where he is currently a Desense Leader.

Jagan Rajagopalan received the master's degree in wireless technology from the University of South Florida, Tampa, FL, USA, in 2010.

He is a Principal RF System Engineer with Wireless Technology Group, Amazon Lab126, Sunnyvale, CA, USA, where he is currently an Engineering Leader. He has 10+ years of work experience in consumer electronics industry. He is the Author of multiple IEEE conference papers and holds multiple U.S. patents in the field of defense, EMI, and RF system design.

Akshay Mohan received the master's degree in wireless technology from the University of Texas, Dallas, TX, USA, in 2013.

He is a Wireless Design Manager with Wireless Technology Group, Amazon Lab126, Sunnyvale, CA, USA.

Donghyun Kim (Member, IEEE) received the B.S., M.S., and Ph.D. degrees in electrical engineering from the Korea Advanced Institute of Science and Technology, Daejeon, South Korea, in 2012, 2014, and 2018, respectively.

In 2018, he joined the Missouri University of Science and Technology (formerly University of Missouri-Rolla), Rolla, MO, USA, and is currently an Assistant Professor with the Missouri S&T EMC Laboratory. His research interests include nanometer-scale devices, through-silicon via technology, dielectric material characterization and signal integrity, power integrity, temperature integrity, electromagnetic compatibility (EMC), and electrostatic discharge in 2.5-D/3-D IC systems.

Dr. Kim was the recipient of the IEEE Region five Outstanding Young Professional (formerly GOLD) Award, IEEE St. Louis Section Outstanding Young Engineer Award, IEEE APEMC Outstanding Young Scientist Award, and DesignCon Best Paper Award, and also the corecipient of the DesignCon Early Career Best Paper Awards and IEEE EMC Symposium Best Paper Awards. He is currently the Vice-Chair of IEEE EMC Society TC-10 (Signal Integrity and Power Integrity) and IEEE St. Louis Section.

Chulsoon Hwang (Senior Member, IEEE) received the B.S., M.S., and Ph.D. degrees in electrical engineering from the Korea Advanced Institute of Science and Technology, Daejeon, South Korea, in 2007, 2009, and 2012, respectively.

From 2012 to 2015, he was a Senior Engineer with Samsung Electronics, Suwon, South Korea. In 2015, he joined the Missouri University of Science and Technology (formerly University of Missouri-Rolla), Rolla, MO, USA, where he is currently an Associate Professor. His research interests include RF desense, signal/power integrity in high-speed digital systems, EMI/EMC, hardware security, and machine learning.

Dr. Hwang was the recipient of the AP-EMC Young Scientist Award, Google Faculty Research Award, and Missouri S&T's Faculty Research Award, and also the corecipient of the seven best paper/best student paper Awards from various conferences including the IEEE EMC+SIPI, AP-EMC, and DesignCon.